PHYSICAL SCIENCES

# Isotope-selective pore opening in a flexible metal-organic framework

**Linda Bondorf[1]†‡, Jhonatan Luiz Fiorio[2]†, Volodymyr Bon[2], Linda Zhang[1], Mariia Maliuta[2], Sebastian Ehrling[2], Irena Senkovska[2], Jack D. Evans[2,3], Jan-Ole Joswig[2], Stefan Kaskel[2]*, Thomas Heine[2,4,5]*, Michael Hirscher[1]***



**Flexible metal-organic frameworks that show reversible guest-induced phase transitions between closed and open pore phases have enormous potential for highly selective, energy-efficient gas separations. Here, we present the gate-opening process of DUT-8(Ni) that selectively responds to $D_2$, whereas no response is observed for $H_2$ and HD. In situ neutron diffraction directly reveals this pressure-dependent phase transition. Low-temperature thermal desorption spectroscopy measurements indicate an outstanding $D_2$-over-$H_2$ selectivity of 11.6 at 23.3 K, with high $D_2$ uptake. First-principles calculations coupled with statistical thermodynamics predict the isotope-selective gate opening, rationalized by pronounced nuclear quantum effects. Simulations suggest DUT-8(Ni) to remain closed in the presence of HT, while it also opens for DT and $T_2$, demonstrating gate opening as a highly effective approach for isotopolog separation.**

## INTRODUCTION

In Earth's crust, deuterium (D or $^2$H), often denoted as "heavy hydrogen," has a very low natural abundance of one deuterium atom per 6500 hydrogen atoms, while the dominant isotope is protium (H or $^1$H) (*1*). Tritium (T or $^3$H) only occurs in traces, produced by cosmic rays or in nuclear power plants. Because of its unique physical properties, deuterium has a broad field of applications ranging from the nuclear industry to specific analytical techniques such as nuclear magnetic resonance (NMR) spectroscopy (*2*), hydrogen deuterium exchange mass spectrometry (*3*), medicine (*4*), drug discovery, and life science (*5*, *6*). Therefore, the demand of pure deuterium and deuterated water is constantly growing since its discovery by Urey *et al.* in 1931 (*7*). The concentration and separation of the deuterium from protium remains an important challenge, and the main industrial techniques are currently limited to energy-demanding chemical exchange, water distillation (*8*), or electrolysis (*9*). In addition to cryogenic distillation, several alternative technologies for H/D separation have been discussed recently: gas chromatography (*10*), palladium-based membranes (*11*), metal-hydride–based techniques (*12*), plasma-chemical methods (*13*), graphene-based membranes (*14*), and layered materials (*15*). Furthermore, the discovery of quantum-sieving effects in confined spaces has opened previously unknown possibilities to use nanoporous solids for isotope separation (*16*).

One class of these nanoporous solids are metal-organic frameworks (MOFs), and the interaction of dihydrogen ($H_2$) with such MOFs has been heavily studied since nearly two decades, see (*17*) and references therein. Large amounts of $H_2$ can be adsorbed in MOFs at low temperature owing to huge specific surface areas, and undercoordinated metal sites can enhance hydrogen adsorption substantially at higher temperatures (*18*, *19*). Moreover, nuclear quantum effects (NQEs) contribute notably to the isotope effect and, as they lower the adsorption enthalpy, restrict their practical application for ambient temperature storage (*20*). Protium has the largest NQE of all isotopes in the periodic table. This is a consequence of being the most light-weight nucleus. The largest mass ratio between isotopes also occurs for hydrogen, leading to a pronounced isotope effect. Compared to other porous materials, MOFs show particularly strong hydrogen isotope selectivities (*21*). This is attributed to two rather different effects: The first is purely kinetic due to the effective molecular radius, where the larger size of $H_2$ prevents its diffusion through the narrow apertures of specific diameter that are present in some MOFs, whereas $D_2$ can penetrate easily (*22*). The second is due to chemical affinity, where strong adsorption sites (typically open metal sites) exhibit a remarkable difference in adsorption enthalpy for the isotopologs, i.e., 2 to 3 kJ mol$^{-1}$ for $H_2$ and $D_2$ (*23*, *24*). This difference results in remarkable separation factors for these isotopologs even at temperatures exceeding 100 K (*24*).

If the MOF is not a static framework but flexible, then it can selectively respond to external stimuli adapting its pore size triggered by adsorption-induced gating or breathing (*25*, *26*). Early reports on gating and breathing were found for [Cu(dhbc)$_2$(4,4′-bpy)] (Hdhbc - 2,5-dihydroxybenzoic acid, 4,4′-bpy - 4,4′-bipyridine) (*27*), Elastic Layered Metal-Organic Framework (ELM-11) (*28*) and Matériaux de l'Institut Lavoisier (MIL-53) (*29*). The transition from a narrow to a large pore in MIL-53 leads to an optimized kinetic quantum sieving between $H_2$ and $D_2$ (*30*). Recent experiments on the same MOF showed a second breathing step, which opens isotope-responsive only with $D_2$ (*31*). In addition, $D_2$ shows a faster interframework diffusivity compared to $H_2$, and this difference counterintuitively increases at higher temperatures (*32*). Another flexible MOF, MUF-15-OMe, shows enhanced kinetic quantum sieving in the pressure-temperature window of the flexible transition (*33*).

The flexible framework DUT-8(Ni) (*34*) is in the focus of the present study. It consists of $Ni_2$ paddle wheels (PWs), 2,6-naphthalenedicarboxylate

[1]Max Planck Institute for Intelligent Systems, Heisenbergstrasse 3, D-70569 Stuttgart, Germany. [2]Technische Universität Dresden, School of Science, Faculty of Chemistry and Food Chemistry, Mommsenstr. 13, 01069 Dresden, Germany. [3]Centre for Advanced Nanomaterials and Department of Chemistry, The University of Adelaide, North Terrace, Adelaide, South Australia 5000, Australia. [4]Helmholtz-Center Dresden-Rossendorf, Leipzig Research Site, Permoserstr. 15, 04138 Leipzig, Germany. [5]Department of Chemistry, Yonsei University, Seodaemun-gu, Seoul 120-749, Republic of Korea.
*Corresponding author. Email: stefan.kaskel@tu-dresden.de (S.K.); thomas.heine@tu-dresden.de (T.H.); hirscher@is.mpg.de (M.H.).
†These authors contributed equally to this work.
‡Present address: German Aerospace Center (DLR), Stuttgart, Germany.

(ndc) linkers and 1,4-diazabicyclo(2.2.2)octane (dabco) pillars forming a primitive cubic net (Fig. 1A). Crystal size, morphology, and conformation are used to effectively tune the responsivity of DUT-8(Ni) (*35*, *36*). While macrosized DUT-8(Ni) crystals show selective guest responsivity associated with a pronounced cell volume change (~250%) upon gate opening [an adsorption-induced transition from a closed-pore (cp) to an open-pore (op) phase triggered by nitrogen, carbon dioxide, or C2-C4 hydrocarbons at their standard boiling points (*37*)], nanocrystals of DUT-8(Ni) are rigid instead and show reversible uptake of gasses after desolvation. This is a behavior typical

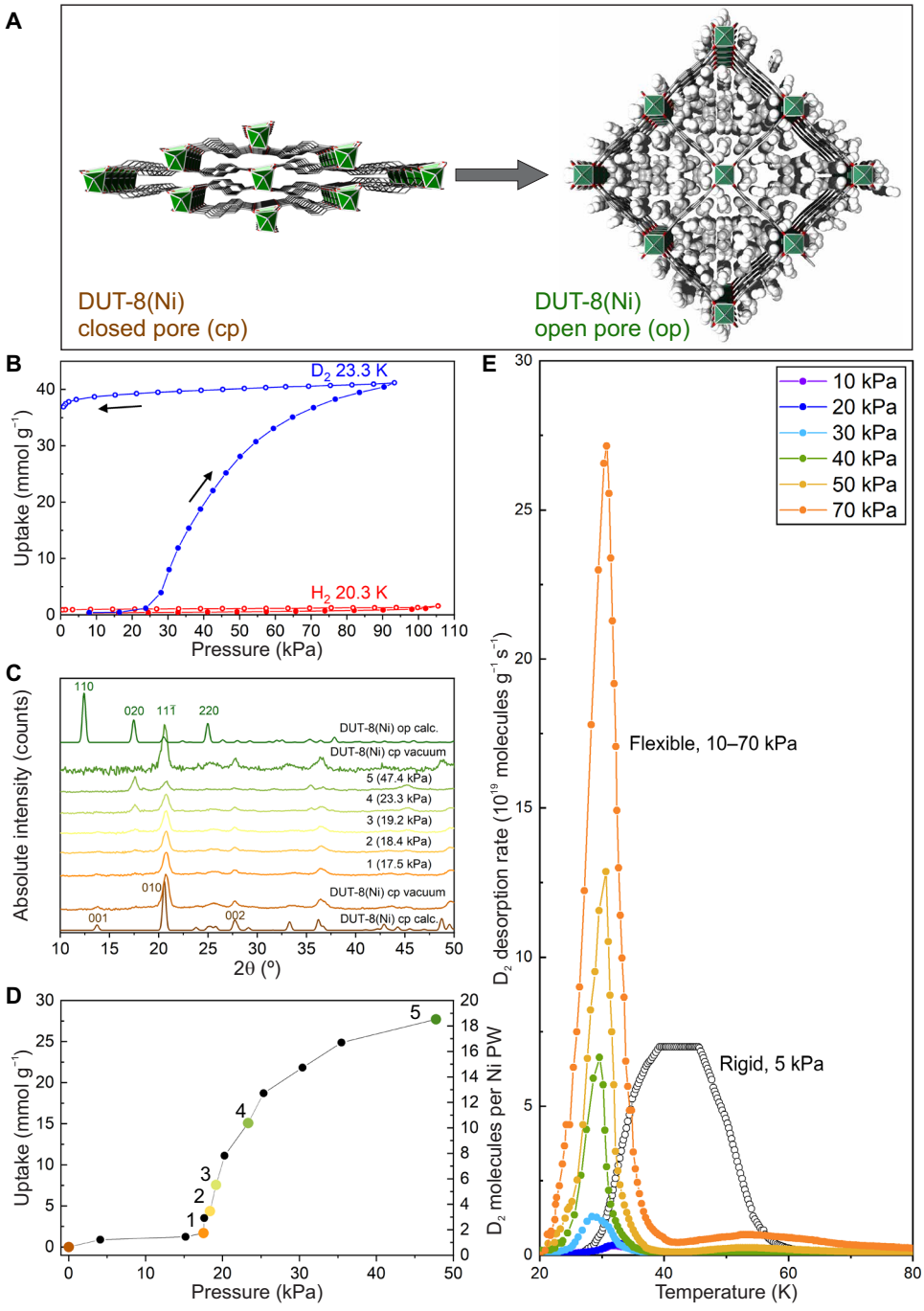


**Fig. 1. Isotope-selective pore opening by deuterium.** (**A**) Crystal structure of DUT-8(Ni) in cp and $D_2$@DUT-8(Ni) op phases ($Ni_2$ PWs are shown as green polyhedra, ndc carbon atoms are shown as gray sticks, and deuterium guest molecules are shown as white spheres). (**B**) $H_2$ and $D_2$ isotherms for DUT-8(Ni) at 20.3 and 23.3 K. Adsorption and desorption curves are measured by a volumetric apparatus with an equilibrium time of 90 min for each isotherm point. (**C**) NPD patterns measured on DUT-8(Ni) at defined pressures in parallel to (**D**) adsorption of $D_2$ at 23.3 K [colors correspond to (D)]. (**E**) TDS with deuterium measured by a home-built cryogenic setup. Measurements of the flexible isomer of DUT-8(Ni) are performed at an exposure temperature of 23.3 K, exposure pressures between 10 and 70 kPa, and an exposure time of 30 min. DUT-8(Ni) rigid is measured after exposure to 5 kPa of deuterium for 10 min at an exposure temperature of 23.3 K. Here, the mass spectrometer reached saturation.

for conventional microporous solids (*38*). The mechanism behind gate opening relies on the hinge energetics of the network nodes, balancing strain energy (favoring the open form) and linker-linker interactions (stabilizing the closed form) (*39*). The guest molecules' interactions with the pore interior counteract these linker-linker interactions and induce gate opening. For gas separation, selective pore opening can induce colossal selectivity (*40*–*43*), which is a key aspect for energy-efficient separation processes (*44*). However, so far, a pore opening in gating MOFs triggered only by protium-free dihydrogen isotopologs has never been reported.

When exposing DUT-8(Ni) to $H_2$, the MOF remains closed. The same is observed when exposing DUT-8(Ni) to the mixed isotopolog HD. In contrast, it readily opens between 23.3 and 26 K upon exposure to $D_2$, where it shows pronounced and reversible gas uptake (Fig. 1B). In this work, we explore this intriguing isotope-triggered structural transition using a wide range of physicochemical methods relying on parallelized adsorption and in situ neutron powder diffraction (NPD), as well as low-temperature thermal desorption spectroscopy (TDS) after exposure to isotope mixtures. First-principles calculations trace back the origin of the isotope-triggered breathing phenomenon to the pronounced NQEs of the adsorbed dihydrogen phase. These calculations are in agreement with the experimental observations for $H_2$, HD, and $D_2$ and predict pore opening for $T_2$ and DT but not for HT.

## RESULTS

### Isotope-selective structural response

Low-temperature adsorption of $H_2$ and $D_2$ gas, each at their standard boiling points, reveals pressure-dependent responsivity toward $D_2$ and $H_2$ (Fig. 1B). The adsorbed amount of $H_2$ is barely above the detection limit with a slight increase up to 1.1 mmol $g^{-1}$ at 100 kPa. Thus, DUT-8(Ni) remains in the cp phase under $H_2$ atmosphere. In stark contrast, after little to no uptake at low pressure, there is steep adsorption of $D_2$ at 24 kPa, the gate-opening pressure resulting in a high-saturation uptake of 41.2 mmol $g^{-1}$ at 100 kPa. The desorption branch indicates a hysteresis as expected for a first-order structural transformation. This isotope-selective host-guest interaction results in a gas uptake of 27 $D_2$ molecules per PW at 100 kPa, whereas only 0.7 $H_2$ molecules are adsorbed on average.

The $D_2$-triggered structural transition from cp to op (cp→op) phase (Fig. 1, A, C, and D, and fig. S4) was confirmed by NPD experiments conducted on DUT-8(Ni) in parallel to the physisorption of $D_2$ at 23.3 K. The NPD patterns, measured in vacuum at 23.3 K, resemble the calculated patterns for DUT-8(Ni) cp. At higher loadings, an additional reflection at $2\theta = 17.7°$ appears in the NPD patterns, indicating the cp→op phase transition in DUT-8(Ni). In the NPD patterns, measured for the loadings 2 to 4 (Fig. 1C), a mixture of cp and op phases is observed, which suggests a sequential switching of individual crystallites. Similar observations were made earlier in the series of powder x-ray diffraction (PXRD) experiments in parallel to adsorption of nitrogen (77 K), *n*-butane (273 K), and carbon dioxide (195 K) (*37*). The most intensive (110) reflection, which is observed at $2\theta = 12.4°$ in the theoretical NPD patterns calculated for the guest-free structure, is suppressed in the experimental patterns measured at a loading of 27 mmol $g^{-1}$. This phenomenon is caused by the ordering of $D_2$ molecules in the channels of DUT-8(Ni) op, which could be captured due to the large coherent scattering length of deuterium for neutrons. The Rietveld refinement of the NPD patterns, measured in vacuum and at 27 mmol $g^{-1}$ $D_2$ loading, approves this hypothesis (figs. S5 and S6). The gate-opening process is reversible: After desorption of $D_2$ in vacuum at 23.3 K, the NPD patterns, which are characteristic for DUT-8(Ni) cp phase, are recovered (Fig. 1C).

To simulate the adsorption-induced cp→op phase transition, grand-canonical Monte Carlo (GCMC) simulations using Feynman-Hibbs quantum effective potentials (*45*) were used (for details, see the Supplementary Materials). The osmotic potential difference $\Delta\Omega_{cp\rightarrow op}$ between both phases (*46*) is shown in Fig. 2C at temperatures of 25, 30, 50, and 70 K. In comparison to other gate-opening MOFs (*47*), DUT-8(Ni) has a relatively large Helmholtz free-energy difference between the op and cp phases ($\Delta F_{cp\rightarrow op}$) that acts to stabilize the cp phase. For example, the Helmholtz free energy is approximately 20 kJ $mol^{-1}$ for MIL-53(Al) (*48*), whereas for DUT-8(Ni), it is 110 kJ $mol^{-1}$. As a result, the dispersion-dominated cp phase requires a remarkable contribution of adsorption potential to produce a phase transition to the op structure. The analysis of $\Delta\Omega_{cp\rightarrow op}$ (Fig. 2C) illustrates very convincingly that low-temperature adsorption (<50 K) can produce favorable energetics of the magnitude required for this transition: At 25 K, the op phase becomes thermodynamically preferred upon $D_2$ adsorption at pressures above 26 kPa. This is in accordance with the experimental observations. In contrast, pressures larger than 60 kPa are required for HD and pressures beyond 190 kPa for $H_2$ to be adsorbed. Thus, these simulations demonstrate how the differences in adsorption enthalpy for $D_2$, HD, and $H_2$ can produce isotope-selective gate opening at these low temperatures.

The $D_2$ adsorption and desorption between 23.3 and 30 K are shown in Fig. 2A. With increasing temperature, the opening pressure increases and the maximal uptake at 100 kPa notably decreases. These changes are most likely related to one another, because a shift to higher opening pressures reduces the pressure range available for inducing the structural transition due to the limiting maximum pressure of the instrument (100 kPa). At a temperature of 30 K, no pore opening occurs below 100 kPa, and the sample remains in the cp phase. Consequently, the breathing of DUT-8(Ni) under subatmospheric $D_2$ pressures is only observed in a narrow temperature range.

The adsorbed $D_2$ amount was analyzed by cryogenic TDS performed in a homebuilt setup (Fig. 1E). After degassing, DUT-8(Ni) was cooled down to 23.3 K and exposed to $D_2$ gas for 30 min. Under high vacuum, the sample was then cooled down to 20 K, followed by constant 0.1 K $s^{-1}$ heating up to 300 K. During heating, the mass spectroscopic data (desorbed gas pressure as a function of time) were collected. Figure 1E shows the evolution of the $D_2$ desorption rate with increasing exposure pressure from 10 to 70 kPa. Up to 20 kPa exposure pressure, the desorption rate, i.e., $D_2$ uptake, is low, because DUT-8(Ni) remains in the cp phase. Starting at 30 kPa—which is above the opening pressure—the desorption peak strongly increases with the exposure pressure. The amount desorbed (area under the desorption peak) is consistently following the pressure dependence observed in the adsorption isotherm (Fig. 1E). The advantage of TDS is the high detection sensitivity allowing measurements on small samples (typical mass around 3 mg) and low gas usage. Therefore, TDS experiments using HD gas are possible for testing if an opening will occur by HD molecules. Figure 2B shows the desorption peaks after exposure to HD in comparison to $H_2$ and $D_2$ for exposure pressures of 1 and 75 kPa at 23.3 K. It clearly indicates that

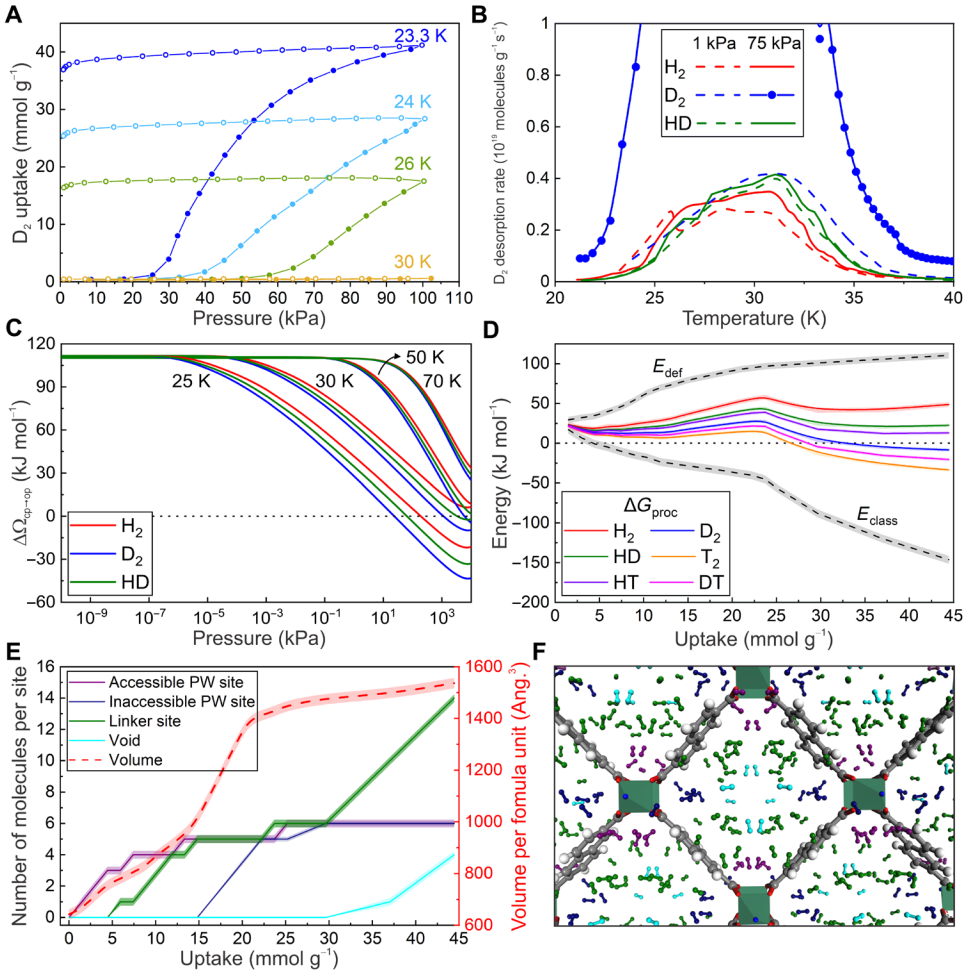


**Fig. 2. Temperature-dependent gate opening for different isotopologs.** (**A**) Temperature-dependent $D_2$ adsorption of DUT-8(Ni): Deuterium isotherms from 30 to 23.3 K. Adsorption and desorption curves are measured with the volumetric instrument, starting at the highest temperature of 30 K and with an equilibrium time of 90 min. (**B**) TDS of DUT-8(Ni) obtained after exposure to 1 and 75 kPa of $H_2$, $D_2$, or HD at 23.3 K for a fixed exposure time ($t_{exp}$) of 10 to 30 min. The desorption spectra after evacuation at exposure temperature were measured for a heating rate of 0.1 K $s^{-1}$. (**C**) Difference in osmotic potential energy for the gate-opening process in DUT-8(Ni) for $H_2$, HD, and $D_2$ at 25, 30, 50, and 70 K, where, for $\Delta\Omega_{cp\rightarrow op} < 0$, the gate opening is thermodynamically favored. (**D**) Gibbs free energies of MOF loading process ($\Delta G_{proc}$) with respect to the unloaded cp DUT-8(Ni) and gas-phase dihydrogen as function of the loading, given for all hydrogen isotopologs, DUT-8(Ni) deformation energy ($E_{def}$) with respect to the cp structure, and the classical adsorption energy ($E_{class}$). The shaded areas give the statistically relevant range, resulting from 50 different configurations. Lines were drawn to guide the eye. (**E**) Distribution of $D_2$ over different adsorption sites in DUT-8(Ni) for increasing loading and pore volume. (**F**) Illustrative representation of the different adsorption sites in DUT-8(Ni). The $D_2$ molecules were colored matching the previous graphic, where there are two PW sites initially accessible (dark blue) and two others inaccessible due to the framework contraction (purple), linker site (green), and void (cyan).

only $D_2$ penetrates DUT-8(Ni) above the opening pressure, whereas no opening occurs for $H_2$ and HD.

To quantify the influence of NQEs and obtain a molecular picture of the adsorption process, density functional theory (DFT) calculations were performed (for details, see the Supplementary Materials). Hereby, the NQEs were considered via the harmonic approximation for the adsorbed guest molecules. Figure 2D shows that none of the isotopologs including protium ($H_2$, HD, or HT) can enter the closed pore, as the corresponding Gibbs adsorption energies are always positive. Opening DUT-8(Ni) cp is an endothermic process with a deformation energy saturating at 110 kJ $mol^{-1}$ for loadings higher than 25 mmol $g^{-1}$ (this corresponds to 15 molecules per PW). Although the classical energy (i.e., no NQEs are considered) favors the adsorption process for loadings beyond 5 mmol $g^{-1}$, NQEs are responsible for an overall unfavorable Gibbs free-energy balance. For loadings beyond 33 mmol $g^{-1}$, the $D_2$-loaded DUT-8(Ni) (and slightly earlier the $T_2$-loaded system) becomes energetically favorable, while the adsorption of the lighter-weight isotopologs $H_2$, HD, and HT remains energetically disfavored. During this hypothetical loading process, different adsorption sites in DUT-8(Ni) are successively occupied (Fig. 2E). First, the accessible low-energy sites at large connector angles (fig. S7) are occupied, followed by the linker sites. This adsorption starts opening the pore. Once it is opened, the connector sites become equivalently accessible, and the remaining two are occupied as well. Only at the final stage of the loading process, the central void of the pore is filled with guest molecules (Fig. 2F).

The DUT-8(Ni) framework can be synthesized as a flexible and rigid form without notable differences in composition (for details, see the Supplementary Materials). The rigidification of flexible MOFs is a consequence of finite size effects (fig. S2) (*38*, *39*, *49*, *50*).

The thermal desorption spectra of the flexible and rigid DUT-8(Ni) material show a clear distinction (Fig. 1E): For an exposure temperature of 23.3 K, the desorption curve of rigid DUT-8(Ni) has a broad maximum between 20 and 75 K centered around 43 ± 5 K. In contrast, the flexible form has a much narrower $D_2$ desorption peak with a maximum at 30 K for exposure above the opening pressure. A desorption maximum at a low temperature usually indicates a small adsorption strength, as less thermal energy is necessary for desorption. In the case of flexible and rigid DUT-8(Ni), the standard interpretation of TDS curves is not applicable due to similar composition and almost identical pore diameters in the op phase. Moreover, the width of the adsorption peak is extraordinarily narrow compared to other TDS measurements on rigid porous structures (*51*). The only plausible explanation is a pore closing of flexible DUT-8(Ni) around 30 K under vacuum in the TDS experiment, which expels the $D_2$ molecules already at low temperature. This is in agreement with temperature-dependent $D_2$ adsorption isotherm measurements on flexible DUT-8(Ni) that show a $D_2$-triggered structural transition only below 30 K (Fig. 2A).

### Selective isotope adsorption of $H_2/D_2$ mixtures

Using cryogenic TDS, hydrogen isotope separation of DUT-8(Ni) can be measured after exposure to a 1:1 $H_2/D_2$ mixture at 23.3 K. After evacuation, the coadsorbed isotopes can be detected simultaneously and quantitatively by the mass spectrometer, which has been previously calibrated according to (*52*). Thus, the $D_2$-over-$H_2$ selectivity can be directly determined from the ratio of the desorbed amounts.

Similar to TDS after pure $D_2$ exposure, the desorption rate shows a narrow maximum for $H_2$ and $D_2$. However, the $D_2$ maximum is much higher indicating a $D_2$ uptake that is approximately 10 times higher than for $H_2$ (Fig. 3A). For exposure at 23.3 K, the average selectivity is 9.9 and, thus, very high at all total exposure pressures (table S1). The $D_2$ uptake increases with exposure pressure and shows the highest value of 9.44 mmol $g^{-1}$ together with the best selectivity of 11.6 after 80 kPa total exposure pressure. This confirms a high separation performance for gas mixtures.

Figure 3B summarizes the results of the $D_2$ and $H_2/D_2$ mixture exposures at 23.3 K measured by TDS and the $D_2$ adsorption isotherm at the same temperature. The gas pressure is correlated to the $D_2$ uptake, which is, in principle, directly proportional to the fraction of opened crystals determined by neutron diffraction. Below 20 kPa, the structure remains closed; then—with increasing pressure—the uptake and, therefore, the fraction of the open phase increase. The similarity of the response between pure $D_2$ gas and $D_2$ partial pressure of the mixture indicates that the DUT-8(Ni) phase transition is driven by the partial pressure of $D_2$ rather than the total gas pressure. Deviations between TDS measurements and the isotherm show that the fraction of the op phase does not only depend on temperature and pressure but also depend on the adsorption kinetics. While for the TDS measurements, each point is a new dosing step for 30-min exposure starting from the fully closed sample; the adsorption isotherm is measured by continuously adding dosing steps, which results in a total exposure time of several hours.

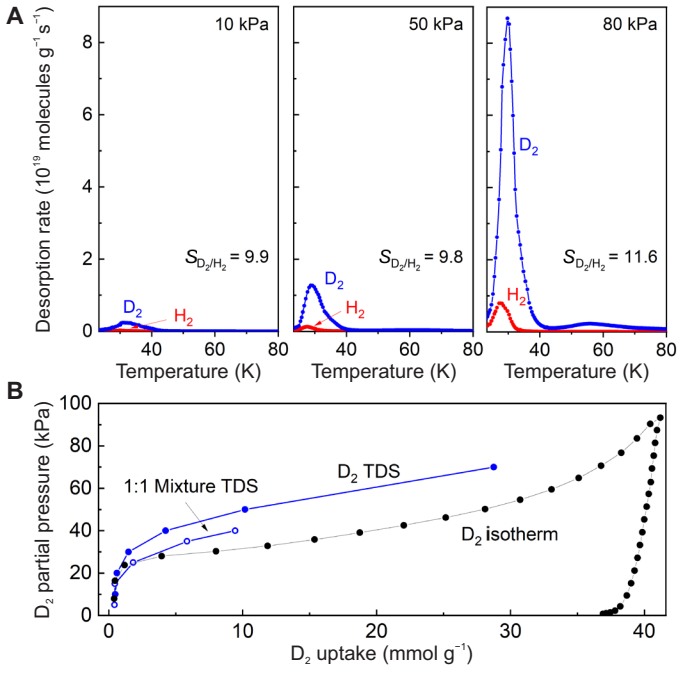


**Fig. 3. Selective isotope adsorption of $H_2/D_2$ mixtures.** (**A**) TDS spectra for DUT-8(Ni) and $D_2/H_2$ selectivities according to the exposed pressure. Measurements were performed under a 1:1 $H_2/D_2$ isotope mixture at 23.3 K for an exposure time of 30 min. (**B**) Applied $D_2$ partial pressure as a function of $D_2$ uptake determined from TDS spectra after 1:1 $H_2$:$D_2$ mixture at 23.3 K compared to $D_2$ uptake in TDS measurements for pure $D_2$ exposure and $D_2$ adsorption isotherms both at 23.3 K.

## DISCUSSION

We found an isotopolog-selective switching mechanism in a flexible framework, demonstrating $D_2$-selective responsivity. The $D_2$-stimulated gate opening at 23.3 K was monitored by parallelized adsorption NPD. Unlike $D_2$, physisorption of $H_2$ or HD shows only negligible adsorption capacity, indicating high selectivity of the framework responsivity toward $D_2$. This high $D_2$ selectivity is explained by DFT calculations, indicating that NQEs are responsible for the unfavorable Gibbs free-energy balance for all isotopologs that contain protium ($H_2$, HD, and HT), whereas all others ($D_2$, DT, and $T_2$) are expected to be adsorbed by DUT-8(Ni) pores under similar conditions. Thermodynamic calculations confirm this finding, indicating that the gate-opening pressure for $D_2$ is shifted toward lower pressures in the adsorption isotherms. A direct comparison of switchable and rigid versions of DUT-8(Ni) via TDS reveals the important advantage of stimuli-responsive frameworks, leading to isotope-selective recognition effects (*53*). The narrow desorption peak centered at 30 K—in combination with high adsorption capacity of 42 mmol $g^{-1}$—represents a unique system advantageous for effective and sustainable isotopolog separation with a narrow temperature swing. This assumption was confirmed in TDS experiments using 1:1 mixture of $D_2$ and $H_2$ and resulted in the excellent selectivity of 11.6 combined with a high $D_2$ uptake of 9.44 mmol $g^{-1}$ ranking DUT-8(Ni) as unique material able to separate $D_2$ from $H_2/D_2$ and even $H_2$/HD/$D_2$ mixtures. Applied for gas separation, porous materials show typically a trade-off between selectivity and adsorption capacity (*54*), which is also observed for hydrogen isotope separation (*55*). For porous materials showing kinetic quantum sieving, the selectivity reaches 10 but the uptake is only 2 mmol $g^{-1}$, while for higher uptake, the selectivity falls below 3; this has been overcome by a special porous organic cage cocrystal with an alternating pore structure reaching a selectivity of 8 and an uptake of 4 mmol $g^{-1}$ (*55*). The

isotope-selective pore opening of DUT-8(Ni) outperforms clearly these materials with permanent porosity and opens a new strategy coping this trade-off problem.

### Outlook

The selective adsorption of protium-free dihydrogen isotopologs offers a path to highly purified heavy hydrogen. Stimuli-responsive MOFs can selectively recognize heavy isotopologs by dynamic pore opening and closing transformations. Understanding the delicate energy balance of a flexible MOF and the dihydrogen adsorption energy subject to strong NQEs opens the possibility to tailor new adsorption materials by rational design, e.g., by linker functionalization, which could, for example, selectively adsorb also HD or HT, but not $H_2$. Although these systems operate only at cryogenic temperatures, the high gas uptake combined with their high selectivity may render these materials as competitive not only compared to cryogenic distillation but also compared to alternative two-dimensional (2D) material–based isotope selective membranes (*14*, *15*).

## MATERIALS AND METHODS

### Synthesis of DUT-8(Ni)

The samples of DUT-8(Ni) flexible and DUT-8(Ni) rigid were synthesized and desolvated according to the procedures reported elsewhere (*38*).

### Characterization of DUT-8(Ni) samples

PXRD patterns were obtained at room temperature on a STOE STADI P diffractometer using Cu-Kα1 radiation (λ = 1.54059 Å) and a 2D detector (Mythen, Dectris). All measurements were performed in transmission geometry using a rotating flatbed sample holder, 2Θ steps scans, with step width of 6° and exposition time of 120 s per step. The measured PXRD patterns (fig. S1A) well match with calculated patterns indicating the phase purity of the powders used in the study.

Volumetric low-pressure nitrogen physisorption experiments at 77 K were conducted on a Quadrasorb apparatus (Quantachrome) using liquid nitrogen as coolant. Helium gas of 99.999% purity was used for determination of the dead volume, and nitrogen gas of 99.999% purity was used as adsorptive. The samples were degassed at 120°C in dynamic vacuum for at least 6 hours before the measurement. The adsorption and desorption isotherms of DUT-8(Ni) flexible and DUT-8(Ni) rigid are shown in fig. S1B. Both isotherms well match with the earlier published data in terms of total uptake in saturation and flexibility behavior for the flexible version, e.g., gate opening and closing pressures (*38*).

### Thermal desorption spectroscopy

Low-temperature TDS experiments have been performed using the setup designed in-house (*56*). After activation, the sample is held under vacuum and cooled down to the exposure temperature. Exposure to different gas atmospheres ($H_2$ from Westfalen AG with purity of 99.999%, $D_2$ from Air Liquide with purity of 99.8%, and HD purchased from Sigma-Aldrich with purity of 96% HD) is conducted for defined exposure times, followed by a 1-min evacuation. Under high vacuum, the sample is then cooled down to 20 K and constantly heated to 300 K with a heating rate of 0.1 K $s^{-1}$. During heating, the mass spectroscopic data, gas pressure as a function of time, are collected to determine the desorption rate of each gas.

For quantitative uptake and selectivity values, the mass spectrometer is calibrated according to (*51*). The calibration alloy $Pd_{95}Ce_5$ is placed under hydrogen or deuterium atmosphere for 2 hours at 1.6 kPa and 353 K. After cooling to room temperature, the amount of loaded gas is weighted. For desorption, the alloy sample is heated up to 600 K with 0.1 K $s^{-1}$. The integral of desorption pressure over time corresponds to the amount of desorbed gas molecules and should be the same as the loaded gas determined by weight. Hence, the ratio of measured weight change to determine gas amount by the desorption integral is used as the specific calibration constant for each gas.

### In situ NPD in parallel to deuterium adsorption at 23 K

In situ NPD experiments were conducted at a neutron powder diffractometer E9-FIREPOD at the BER II neutron source of the Helmholtz-Zentrum Berlin using incoming neutrons with wavelength λ = 2.8172(2) Å (*57*). A cylindrically shaped aluminum sample holder with an inner diameter of 1 cm and a length of 12 cm was filled and sealed under argon atmosphere with 860 mg of DUT-8(Ni) flexible. The sample holder was connected to a gas handling system via a stainless-steel capillary that allowed controlled dosing of deuterium in the pressure range of 0.001 to 100 kPa with a homemade apparatus. The sample was cooled by a closed-cycle helium cryostat system, and the temperature was monitored directly at the sample cell by the silicone diode (accuracy, ±0.1 K) connected to a Lakeshore 340 temperature controller. Before the NPD measurement, the samples were outgassed in dynamic vacuum (<0.1 Pa) at 298 K for at least 1 hour. Afterward, the samples were cooled to 23.3 K, and the NPD of the guest-free evacuated MOF was recorded. The calibrated standard volumes of the gas handling system and dead volume of the measuring cell allowed to exactly reproduce the ex situ measured isotherm (fig. S4A) and collect NPD patterns at the points of interest (fig. S4B). Each NPD pattern was measured for 12 hours in the range of 2θ = 4° to 140°. The reflections from the aluminum sample can are marked with asterisks. The qualitative analysis of in situ dataset suggests the similar adsorption behavior of deuterium on DUT-8(Ni) at 23.3 K as it was earlier observed in ex situ experiments. The shift of the gate-opening pressure toward lower absolute pressures can be explained by the minor difference in the temperature and, in particular, by much longer adsorption equilibrium times up to 12 hours in the case of the isotherm measured in situ. Analysis of the NPD patterns suggests the mechanism of "gate opening" for deuterium-induced DUT-8(Ni) similar to that observed for nitrogen, carbon dioxide, and hydrocarbons at corresponding standard boiling points (*37*). The mixture of cp and op phases observed in the NPD patterns measured in the gate suggests the low sequential switching of individual crystallites.

### Rietveld refinement of DUT-8(Ni) closed and open phases from the NPD data

A detailed analysis of the NPD data (fig. S4b) shows that patterns measured on the degassed DUT-8(Ni) sample well match with the theoretical patterns generated for DUT-8(Ni) cp. However, NPD patterns measured on $D_2$-loaded samples displayed a considerable mismatch to the theoretical NPD patterns calculated for the guest-free DUT-8(Ni) op, namely, the most intensive reflection (110) calculated at 2θ = 12.4° is not observed in the experimental NPD patterns even at higher loadings. Because of the high coherent scattering length of deuterium, which is comparable with $^{12}C$, the

influence of the ordered guests in the channels of DUT-8(Ni) could strongly influence the reflection intensities in NPD patterns. To prove this hypothesis, NPD patterns of degassed DUT-8(Ni) cp and NPD patterns measured at the loading of 27 mmol $g^{-1}$ were subjected to the Rietveld analysis (figs. S5 and S6). The structures were refined using a Reflex tool in the Materials Studio 5.0 software (Accelrys Software Inc., San Diego, USA). The initial model for cp phase used in the refinement was obtained from Bon *et al.* (*37*), and the structure of the monoclinic conformer of DUT-8(Ni) op was obtained from Petkov *et al.* (*39*). Because of a low data-to-parameter ratio, a rigid body refinement with energy option (energy contribution 1%) was performed for the refinement of the DUT-8(Ni) cp structure. Nickel atoms, naphthalene cores, dabco ligands, and carboxylates were treated as independent rigid fragments of the structure. During the refinement of the DUT-8(Ni) op structure, 18 $D_2$ molecules per Ni PW were inserted in the pores and refined as rigid moieties without energy restrictions. In both cases, similar convergence factors could be reached indicating the correctness of the obtained structural models.

### Density functional calculations

All calculations were carried out using DFT using the Perdew–Burke-Ernzerhof (PBE) functional (*58*), Goedecker-Teter-Hutter pseudopotentials (*59*) incorporating scalar-relativistic core corrections and D3 London dispersion corrections (*60*), together with a triple-zeta valence with two sets of polarization functions (TZVPP) basis set, with a grid cutoff of 400 Ry for geometry optimization, as implemented in the QUICKSTEP (*61*) module of the CP2K program package (*62*).

Periodic DUT-8(Ni) structures were loaded successively with $H_2$ molecules starting from the close-pore structure. For each loading, random positions and orientations of the guest molecules were generated using the Packmol code (*63*). A full geometry optimization of the periodic cell and the atomic positions led to adjustment of the pore size and the occupation of favorable adsorption sites to the respective filling. Moreover, averaging over results of 50 independent, randomly generated starting configurations for each loading eliminated possible influence of initial structures.

A frequency analysis of each optimized geometry was performed within the harmonic approximation. The zero-point energy (ZPE) correction per adsorbed molecule was calculated according to $E_{\mathrm{ZPE,mol}} = \frac{1}{2}\sum h c \bar{\nu}_i$ following the approach of Sillar *et al.* (*64*). This term differs for the dihydrogen isotopologs ($H_2$, $D_2$, and HD) due to their mass differences. The respective ZPE correction term was added to the zero Kelvin total energy values, which are equal for the different hydrogen isotopologs. The frequencies of all adsorbed molecules were used for the ZPE correction of the loaded MOF, whereas the ZPE of a single gas molecule was scaled to the loading to account for the ZPE correction of the free gas-phase molecules.

The ZPE-corrected process adsorption energy $\Delta U_{\mathrm{proc}}$ (per PW) was calculated from the following contributions: (i) the ZPE-corrected total energy of the optimized MOF loaded with $n$ $H_2$ molecules ($U_{n\mathrm{H2\,@\,MOF}n}$), (ii) the ZPE-corrected total energy of the close-pore MOF structure ($U_{\mathrm{MOF0}}$), and (iii) the ZPE-corrected total energy of a single gas-phase $H_2$ molecule multiplied with the number of molecules present in the structure ($nU_{\mathrm{H2}}$): $\Delta U_{\mathrm{proc}} = U_{n\mathrm{H2\,@\,MOF}n} - (U_{\mathrm{MOF0}} + nU_{\mathrm{H2}})$. The same approach was used for the other dihydrogen isotopologs ($D_2$, HD, etc.).

Thermal corrections to the process adsorption energy $\Delta U_{\mathrm{proc}}$ were considered according to $G = U - TS^{\mathrm{vib}}$ to result the process Gibbs free energy $\Delta G_{\mathrm{proc}}$. Thereby, $U$ was obtained as explained above, the temperature was set to 23 K, and $S^{\mathrm{vib}}$ was calculated by considering the product of the individual contributions of each of the six normal modes involved in the vibrational partition function $S^{\mathrm{vib}} = Nk_{\mathrm{B}}\sum[\Theta_i^{\mathrm{vib}}T^{-1}(e^{+\Theta_i^{\mathrm{vib}}/T}-1)^{-1} - \ln(1-e^{-\Theta_i^{\mathrm{vib}}/T})]$ with the characteristic vibrational temperature defined as $\Theta_i^{\mathrm{vib}} = \frac{hc\bar{\nu}_i}{k_{\mathrm{B}}}$.

Figure S7 schematically illustrates the gate-opening process through adsorption of guest molecules at different adsorption sites. Initially, only two connector sites (violet area) are accessible to guest molecules (cf. Fig. 2E). These accessible PW sites are occupied first, whereby the pore is slightly opened making the linker sites (green area) accessible for adsorption. Further opening results in adsorption at the initially inaccessible PW sites (dark blue area), and last, the inner void of the pore (light blue area) is occupied by guest molecules.

### GCMC simulations

GCMC simulations were performed using the RASPA 2.0 software (*65*). The structure of the DFT-optimized op phase as a 2 × 2 × 3 supercell was used. The model proposed by Levesque and co-workers (*66*) was used to treat dihydrogen isotopologs. This model describes hydrogen as a rigid three-site molecule with the H—H bond length fixed at 0.74 Å and partial atomic charges placed at the two hydrogen atom sites and at the center of mass to reproduce the quadrupole moment of molecular hydrogen. To describe the potential energy, the OPLS-AA force field (*67*) was used to assign the intramolecular interactions of the framework, and the parameters were computed with the Lorentz-Berthelot combining rules. Partial atomic charges were assigned using the restrained electrostatic potential method based on the DFT calculations (*68*). To account for quantum effects in the Monte-Carlo simulations, the Feynman-Hibbs correction to the Lennard-Jones potential (*45*) was applied

$$U(r_{ij}) = 4\varepsilon_{ij}\left[\left(\frac{\sigma_{ij}}{r_{ij}}\right)^{12} - \left(\frac{\sigma_{ij}}{r_{ij}}\right)^{6}\right] + \frac{4\varepsilon_{ij}}{r_{ij}^2}\frac{\hbar^2}{24\mu_{ij}k_{\mathrm{B}}T}\left[132\left(\frac{\sigma_{ij}}{r_{ij}}\right)^{12} - 30\left(\frac{\sigma_{ij}}{r_{ij}}\right)^{6}\right]$$

Monte-Carlo moves included insertion, deletion, translation, rotation, and reinsertion. A 10,000-cycle equilibration period followed by a 100,000-cycle production run was used to obtain converged quantities. Widom insertion simulations (*69*) were used to compute the adsorption enthalpy and the Henry coefficient using 100,000-cycle equilibration and production periods.

The osmotic potential energy $\Delta\Omega_{\mathrm{cp}\rightarrow\mathrm{op}}$ to describe the gate-opening process (*46*) was calculated using

$$\Delta\Omega_{\mathrm{cp}\rightarrow\mathrm{op}}(T,P) = \Delta F_{\mathrm{cp}\rightarrow\mathrm{op}} + P\Delta V_{\mathrm{cp}\rightarrow\mathrm{op}} - \int_0^P N_{\mathrm{op}}(p,T)\,V_{\mathrm{m}}(p,T)\,\mathrm{d}p$$

where the Helmholtz energy $\Delta F_{\mathrm{cp}\rightarrow\mathrm{op}}$ was approximated from DFT calculations by the quasi-harmonic approximation used by the Phonopy code (*70*).

## SUPPLEMENTARY MATERIALS

Supplementary material for this article is available at https://science.org/doi/10.1126/sciadv.abn7035

## REFERENCES AND NOTES

1. B. Zohuri, *Hydrogen energy, Challenges and Solutions for a Cleaner Future/Bahman Zohuri* (Springer, 2019).
2. V. Tugarinov, V. Kanelis, L. E. Kay, Isotope labeling strategies for the study of high-molecular-weight proteins by solution NMR spectroscopy. *Nat. Protoc.* **1**, 749–754 (2006).

3. G. R. Masson, J. E. Burke, N. G. Ahn, G. S. Anand, C. Borchers, S. Brier, G. M. Bou-Assaf, J. R. Engen, S. W. Englander, J. Faber, R. Garlish, P. R. Griffin, M. L. Gross, M. Guttman, Y. Hamuro, A. J. R. Heck, D. Houde, R. E. Iacob, T. J. D. Jørgensen, I. A. Kaltashov, J. P. Klinman, L. Konermann, P. Man, L. Mayne, B. D. Pascal, D. Reichmann, M. Skehel, J. Snijder, T. S. Strutzenberg, E. S. Underbakke, C. Wagner, T. E. Wales, B. T. Walters, D. D. Weis, D. J. Wilson, P. L. Wintrode, Z. Zhang, J. Zheng, D. C. Schriemer, K. D. Rand, Recommendations for performing, interpreting and reporting hydrogen deuterium exchange mass spectrometry (HDX-MS) experiments. *Nat. Methods* **16**, 595–602 (2019).
4. T. Pirali, M. Serafini, S. Cargnin, A. A. Genazzani, Applications of deuterium in medicinal chemistry. *J. Med. Chem.* **62**, 5276–5297 (2019).
5. T. G. Gant, Using deuterium in drug discovery: Leaving the label in the drug. *J. Med. Chem.* **57**, 3595–3611 (2014).
6. J. Atzrodt, V. Derdau, W. J. Kerr, M. Reid, Deuterium- and tritium-labelled compounds: Applications in the life sciences. *Angew. Chem. Int. Ed. Engl.* **57**, 1758–1784 (2018).
7. H. C. Urey, F. G. Brickwedde, G. M. Murphy, A hydrogen isotope of mass 2. *Phys. Rev.* **39**, 164–165 (1932).
8. H. Craig, L. I. Gordon, Y. Horibe, Isotopic exchange effects in the evaporation of water: 1. Low-temperature experimental results. *J. Geophys. Res.* **68**, 5079–5087 (1963).
9. H. K. Rae, in *Separation of Hydrogen Isotopes*, H. K. Rae, Ed. (American Chemical Society, 1978), vol. 68, pp. 1–26.
10. W. A. van Hook, in *Isotope Effects in Chemical Processes*, W. Spindel, Ed. (American Chemical Society, 1969), vol. 89, pp. 99–118.
11. D. J. Haynes, B. H. Howard, D. Shekhawat, N. C. Means, *Hydrogen Isotope Separation By a Palladium-Based Membrane* (2019); www.aiche.org/conferences/aiche-annual-meeting/2019/proceeding/paper/559ac-hydrogen-isotope-separation-palladium-based-membrane.
12. A. H. Horen, M. W. Lee, *Metal Hydride Based Isotope Separation - Large-Scale Operations* (Westinghouse Savannah River Company, 1991).
13. I. G. KOO, W. M. LEE, Hydrogen isotope separation by plasma-chemical method. *J. Nuclear Sci. Technol.* **42**, 717–723 (2005).
14. M. Lozada-Hidalgo, S. Hu, O. Marshall, A. Mishchenko, A. N. Grigorenko, R. A. W. Dryfe, B. Radha, I. V. Grigorieva, A. K. Geim, Sieving hydrogen isotopes through two-dimensional crystals. *Science* **351**, 68–70 (2016).
15. S. Hu, K. Gopinadhan, A. Rakowski, M. Neek-Amal, T. Heine, I. V. Grigorieva, S. J. Haigh, F. M. Peeters, A. K. Geim, M. Lozada-Hidalgo, Transport of hydrogen isotopes through interlayer spacing in van der Waals crystals. *Nat. Nanotechnol.* **13**, 468–472 (2018).
16. J. Beenakker, V. D. Borman, S. Krylov, Molecular transport in subnanometer pores: Zero-point energy, reduced dimensionality and quantum sieving. *Chem. Phys. Lett.* **232**, 379–382 (1995).
17. M. P. Suh, H. J. Park, T. K. Prasad, D.-W. Lim, Hydrogen storage in metal-organic frameworks. *Chem. Rev.* **112**, 782–835 (2012).
18. M. Dincă, J. R. Long, Hydrogen storage in microporous metal–organic frameworks with exposed metal sites. *Angew. Chem. Int. Ed. Engl.* **47**, 6766–6779 (2008).
19. Z. Chen, P. Li, R. Anderson, X. Wang, X. Zhang, L. Robison, L. R. Redfern, S. Moribe, T. Islamoglu, D. A. Gómez-Gualdrón, T. Yildirim, J. F. Stoddart, O. K. Farha, Balancing volumetric and gravimetric uptake in highly porous materials for clean energy. *Science* **368**, 297–303 (2020).
20. M. Wahiduzzaman, C. F. J. Walther, T. Heine, Hydrogen adsorption in metal-organic frameworks: The role of nuclear quantum effects. *J. Chem. Phys.* **141**, 064708 (2014).
21. J. Y. Kim, H. Oh, H. R. Moon, Hydrogen isotope separation in confined nanospaces: Carbons, zeolites, metal–organic frameworks, and covalent organic frameworks. *Adv. Mater.* **31**, e1805293 (2019).
22. J. Teufel, H. Oh, M. Hirscher, M. Wahiduzzaman, L. Zhechkov, A. Kuc, T. Heine, D. Denysenko, D. Volkmer, MFU-4 – a metal-organic framework for highly effective $H_2/D_2$ separation. *Adv. Mater.* **25**, 635–639 (2013).
23. H. Oh, I. Savchenko, A. Mavrandonakis, T. Heine, M. Hirscher, Highly effective hydrogen isotope separation in nanoporous metal-organic frameworks with open metal sites: Direct measurement and theoretical analysis. *ACS Nano* **8**, 761–770 (2014).
24. I. Weinrauch, I. Savchenko, D. Denysenko, S. M. Souliou, H.-H. Kim, M. Le Tacon, L. L. Daemen, Y. Cheng, A. Mavrandonakis, A. J. Ramirez-Cuesta, D. Volkmer, G. Schütz, M. Hirscher, T. Heine, Capture of heavy hydrogen isotopes in a metal-organic framework with active Cu(I) sites. *Nat. Commun.* **8**, 14496 (2017).
25. A. Schneemann, V. Bon, I. Schwedler, I. Senkovska, S. Kaskel, R. A. Fischer, Flexible metal-organic frameworks. *Chem. Soc. Rev.* **43**, 6062–6096 (2014).
26. S. Krause, N. Hosono, S. Kitagawa, Chemistry of soft porous crystals: Structural dynamics and gas adsorption properties. *Angew. Chem. Int. Ed. Engl.* **59**, 15325–15341 (2020).
27. R. Kitaura, K. Seki, G. Akiyama, S. Kitagawa, Porous coordination-polymer crystals with gated channels specific for supercritical gases. *Angew. Chem. Int. Ed. Engl.* **42**, 428–431 (2003).
28. D. Li, K. Kaneko, Hydrogen bond-regulated microporous nature of copper complex-assembled microcrystals. *Chem. Phys. Lett.* **335**, 50–56 (2001).
29. T. K. Trung, P. Trens, N. Tanchoux, S. Bourrelly, P. L. Llewellyn, S. Loera-Serna, C. Serre, T. Loiseau, F. Fajula, G. Férey, Hydrocarbon adsorption in the flexible metal organic frameworks MIL-53(Al, Cr). *J. Am. Chem. Soc.* **130**, 16926–16932 (2008).
30. J. Y. Kim, L. Zhang, R. Balderas-Xicohténcatl, J. Park, M. Hirscher, H. R. Moon, H. Oh, Selective hydrogen isotope separation via breathing transition in MIL-53(Al). *J. Am. Chem. Soc.* **139**, 17743–17746 (2017).
31. J. Y. Kim, J. Park, J. Ha, M. Jung, D. Wallacher, A. Franz, R. Balderas-Xicohténcatl, M. Hirscher, S. G. Kang, J. T. Park, I. H. Oh, H. R. Moon, H. Oh, Specific isotope-responsive breathing transition in flexible metal-organic frameworks. *J. Am. Chem. Soc.* **142**, 13278–13282 (2020).
32. M. Jung, J. Park, R. Muhammad, J. Y. Kim, V. Grzimek, M. Russina, H. R. Moon, J. T. Park, H. Oh, Elucidation of diffusivity of hydrogen isotopes in flexible MOFs by quasi-elastic neutron scattering. *Adv. Mater.* **33**, e2007412 (2021).
33. O. T. Qazvini, V.-J. Scott, L. Bondorf, M. Ducamp, M. Hirscher, F.-X. Coudert, S. G. Telfer, Flexibility of a metal–organic framework enhances gas separation and enables quantum sieving. *Chem. Mater.* **33**, 8886–8894 (2021).
34. N. Klein, C. Herzog, M. Sabo, I. Senkovska, J. Getzschmann, S. Paasch, M. R. Lohe, E. Brunner, S. Kaskel, Monitoring adsorption-induced switching by $^{129}$Xe NMR spectroscopy in a new metal-organic framework $Ni_2$(2,6-ndc)$_2$(dabco). *Phys. Chem. Chem. Phys.* **12**, 11778–11784 (2010).
35. S. Ehrling, E. M. Reynolds, V. Bon, I. Senkovska, T. E. Gorelik, J. D. Evans, M. Rauche, M. Mendt, M. S. Weiss, A. Pöppl, E. Brunner, U. Kaiser, A. L. Goodwin, S. Kaskel, Adaptive response of a metal-organic framework through reversible disorder-disorder transitions. *Nat. Chem.* **13**, 568–574 (2021).
36. L. Abylgazina, I. Senkovska, R. Engemann, S. Ehrling, T. E. Gorelik, N. Kavoosi, U. Kaiser, S. Kaskel, Impact of crystal size and morphology on switchability characteristics in pillared-layer metal-organic framework DUT-8(Ni). *Front. Chem.* **9**, 674566 (2021).
37. V. Bon, N. Klein, I. Senkovska, A. Heerwig, J. Getzschmann, D. Wallacher, I. Zizak, M. Brzhezinskaya, U. Mueller, S. Kaskel, Exceptional adsorption-induced cluster and network deformation in the flexible metal-organic framework DUT-8(Ni) observed by in situ x-ray diffraction and EXAFS. *Phys. Chem. Chem. Phys.* **17**, 17471–17479 (2015).
38. N. Kavoosi, V. Bon, I. Senkovska, S. Krause, C. Atzori, F. Bonino, J. Pallmann, S. Paasch, E. Brunner, S. Kaskel, Tailoring adsorption induced phase transitions in the pillared-layer type metal-organic framework DUT-8(Ni). *Dalton Trans.* **46**, 4685–4695 (2017).
39. P. S. Petkov, V. Bon, C. L. Hobday, A. B. Kuc, P. Melix, S. Kaskel, T. Düren, T. Heine, Conformational isomerism controls collective flexibility in metal-organic framework DUT-8(Ni). *Phys. Chem. Chem. Phys.* **21**, 674–680 (2019).
40. M. L. Foo, R. Matsuda, Y. Hijikata, R. Krishna, H. Sato, S. Horike, A. Hori, J. Duan, Y. Sato, Y. Kubota, M. Takata, S. Kitagawa, An adsorbate discriminatory gate effect in a flexible porous coordination polymer for selective adsorption of CO2 over C2H2. *J. Am. Chem. Soc.* **138**, 3022–3030 (2016).
41. H. Sato, W. Kosaka, R. Matsuda, A. Hori, Y. Hijikata, R. V. Belosludov, S. Sakaki, M. Takata, S. Kitagawa, Self-accelerating CO sorption in a soft nanoporous crystal. *Science* **343**, 167–170 (2014).
42. L. Li, R.-B. Lin, R. Krishna, X. Wang, B. Li, H. Wu, J. Li, W. Zhou, B. Chen, Flexible-robust metal–organic framework for efficient removal of propyne from propylene. *J. Am. Chem. Soc.* **139**, 7733–7736 (2017).
43. A. Knebel, B. Geppert, K. Volgmann, D. I. Kolokolov, A. G. Stepanov, J. Twiefel, P. Heitjans, D. Volkmer, J. Caro, Defibrillation of soft porous metal-organic frameworks with electric fields. *Science* **358**, 347–351 (2017).
44. D. S. Sholl, R. P. Lively, Seven chemical separations to change the world. *Nature* **532**, 435–437 (2016).
45. L. M. Sesé, Feynman-Hibbs potentials and path integrals for quantum Lennard-Jones systems: Theory and Monte Carlo simulations. *Mol. Phys.* **85**, 931–947 (1995).
46. F.-X. Coudert, M. Jeffroy, A. H. Fuchs, A. Boutin, C. Mellot-Draznieks, Thermodynamics of guest-induced structural transitions in hybrid organic-inorganic frameworks. *J. Am. Chem. Soc.* **130**, 14294–14302 (2008).
47. J. Wieme, K. Lejaeghere, G. Kresse, V. van Speybroeck, Tuning the balance between dispersion and entropy to design temperature-responsive flexible metal-organic frameworks. *Nat. Commun.* **9**, 4899 (2018).
48. R. Demuynck, S. M. J. Rogge, L. Vanduyfhuys, J. Wieme, M. Waroquier, V. van Speybroeck, Efficient construction of free energy profiles of breathing metal-organic frameworks using advanced molecular dynamics simulations. *J. Chem. Theory Comput.* **13**, 5861–5873 (2017).
49. J. Y. Lee, L. Pan, X. Huang, T. J. Emge, J. Li, A systematic approach to building highly porous, noninterpenetrating metal-organic frameworks with a large capacity for adsorbing H2 and CH4. *Adv. Funct. Mater.* **21**, 993–998 (2011).
50. S. Ehrling, H. Miura, I. Senkovska, S. Kaskel, From macro- to nanoscale: Finite size effects on metal–organic framework switchability. *Trends Chem.* **3**, 291–304 (2021).
51. I. Krkljus, M. Hirscher, Characterization of hydrogen/deuterium adsorption sites in nanoporous Cu–BTC by low-temperature thermal-desorption mass spectroscopy. *Microporous Mesoporous Mater.* **142**, 725–729 (2011).

52. F. von Zeppelin, M. Haluška, M. Hirscher, Thermal desorption spectroscopy as a quantitative tool to determine the hydrogen content in solids. *Thermochim. Acta* **404**, 251–258 (2003).
53. A. P. Katsoulidis, D. Antypov, G. F. S. Whitehead, E. J. Carrington, D. J. Adams, N. G. Berry, G. R. Darling, M. S. Dyer, M. J. Rosseinsky, Chemical control of structure and guest uptake by a conformationally mobile porous material. *Nature* **565**, 213–217 (2019).
54. N. Kumar, S. Mukherjee, N. C. Harvey-Reid, A. A. Bezrukov, K. Tan, V. Martins, M. Vandichel, T. Pham, L. M. van Wyk, K. Oyekan, A. Kumar, K. A. Forrest, K. M. Patil, L. J. Barbour, B. Space, Y. Huang, P. E. Kruger, M. J. Zaworotko, Breaking the trade-off between selectivity and adsorption capacity for gas separation. *Chem* **7**, 3085–3098 (2021).
55. M. Liu, L. Zhang, M. A. Little, V. Kapil, M. Ceriotti, S. Yang, L. Ding, D. L. Holden, R. Balderas-Xicohténcatl, D. He, R. Clowes, S. Y. Chong, G. Schütz, L. Chen, M. Hirscher, A. I. Cooper, Barely porous organic cages for hydrogen isotope separation. *Science* **366**, 613–620 (2019).
56. B. Panella, M. Hirscher, B. Ludescher, Low-temperature thermal-desorption mass spectroscopy applied to investigate the hydrogen adsorption on porous materials. *Microporous Mesoporous Mater.* **103**, 230–234 (2007).
57. A. Franz, A. Hoser, E9: The fine-resolution powder diffractometer (FIREPOD) at BER II. *J. Large Scale Res. Facilities* **3**, 103 (2017).
58. J. P. Perdew, K. Burke, M. Ernzerhof, Generalized gradient approximation made simple. *Phys. Rev. Letters* **77**, 3865–3868 (1996).
59. S. Goedecker, M. Teter, J. Hutter, Separable dual-space Gaussian pseudopotentials. *Phys. Rev. B Conden. Matter* **54**, 1703–1710 (1996).
60. S. Grimme, J. Antony, S. Ehrlich, H. Krieg, A consistent and accurate ab initio parametrization of density functional dispersion correction (DFT-D) for the 94 elements H-Pu. *J. Chem. Phys.* **132**, 154104 (2010).
61. J. VandeVondele, M. Krack, F. Mohamed, M. Parrinello, T. Chassaing, J. Hutter, Quickstep: Fast and accurate density functional calculations using a mixed Gaussian and plane waves approach. *Comput. Phys. Commun.* **167**, 103–128 (2005).
62. G. Lippert, J. Hutter, M. Parrinello, A hybrid Gaussian and plane wave density functional scheme. *Mol. Phys.* **92**, 477–488 (1997).
63. L. Martínez, R. Andrade, E. G. Birgin, J. M. Martínez, PACKMOL: A package for building initial configurations for molecular dynamics simulations. *J. Comput. Chem.* **30**, 2157–2164 (2009).
64. K. Sillar, A. Hofmann, J. Sauer, Ab initio study of hydrogen adsorption in MOF-5. *J. Am. Chem. Soc.* **131**, 4143–4150 (2009).
65. D. Dubbeldam, S. Calero, D. E. Ellis, R. Q. Snurr, RASPA: Molecular simulation software for adsorption and diffusion in flexible nanoporous materials. *Mol. Simul.* **42**, 81–101 (2016).
66. D. Levesque, A. Gicquel, F. L. Darkrim, S. B. Kayiran, Monte Carlo simulations of hydrogen storage in carbon nanotubes. *J. Phys. Condens. Matter* **14**, 9285–9293 (2002).
67. W. L. Jorgensen, D. S. Maxwell, J. Tirado-Rives, Development and testing of the OPLS all-atom force field on conformational energetics and properties of organic liquids. *J. Am. Chem. Soc.* **118**, 11225–11236 (1996).
68. D. Golze, J. Hutter, M. Iannuzzi, Wetting of water on hexagonal boron nitride@Rh(111): A QM/MM model based on atomic charges derived for nano-structured substrates. *Phys. Chem. Chem. Phys.* **17**, 14307–14316 (2015).
69. D. Frenkel, B. Smit, *Understanding Molecular Simulation*, *From Algorithms to Applications* (Acad. Press, ed. 2, 2009).
70. A. Togo, I. Tanaka, First principles phonon calculations in materials science. *Scr. Mater.* **108**, 1–5 (2015).


**Acknowledgments:** In situ NPD measurements were carried out at a fine-resolution powder diffractometer E9 (FIREPOD) at the BER II research reactor operated by the Helmholtz-Zentrum Berlin für Materialien und Energie. D. Wallacher, A. Franz, and N. Grimm are acknowledged for support during the in situ NPD measurements. We thank N. Bönisch for acquiring scanning electron microscopy images and R. Balderas-Xicohténcatl for support during adsorption experiments. **Funding:** The current study was funded by DFG within FOR2433 research unit "MOF-switches." V.B. thanks BMBF (project no. 05K19OD2) for financial support. J.D.E. is supported by a Ramsay Fellowship from the University of Adelaide. T.H. thanks DFG RTG2721 "Hydrogen Isotopes." ZIH Dresden and Phoenix HPC service at the University of Adelaide are thanked for providing high-performance computing resources. **Author contributions:** L.B., I.S., M.H., and T.H. conceived the project. M.M. and S.E. performed the synthesis and standard characterization of MOFs. L.B. performed adsorption and TDS experiments with hydrogen and deuterium under the guidance of M.H. V.B. conducted in situ NPD in parallel to deuterium physisorption and analyzed the data. L.Z. conducted TDS measurements with HD. J.L.F. performed the DFT and thermodynamic calculations under the guidance of J.-O.J. and T.H. The osmotic pressure calculations were contributed by J.D.E.. All authors contributed in analyzing the data and writing the manuscript. **Competing interests:** The authors declare that they have no competing interests. **Data and materials availability:** All data needed to evaluate the conclusions in the paper are present in the paper and/or the Supplementary Materials. Raw data can be found at the Zenodo repository (doi: 10.5281/zenodo.6010408).

Submitted 14 December 2021
Accepted 23 February 2022
Published 13 April 2022
10.1126/sciadv.abn7035